

LARGE MAGELLANIC CLOUD NEAR-INFRARED SYNOPTIC SURVEY. IV.  
LEAVITT LAWS FOR TYPE II CEPHEID VARIABLES

ANUPAM BHARDWAJ,<sup>1,2</sup> LUCAS M. MACRI,<sup>3</sup> MARINA REJKUBA,<sup>2</sup> SHASHI M. KANBUR,<sup>4</sup> CHOW-CHOONG NGEOW,<sup>5</sup> AND  
HARINDER P. SINGH<sup>1</sup>

<sup>1</sup>*Department of Physics & Astrophysics, University of Delhi, Delhi 110007, India*

<sup>2</sup>*European Southern Observatory, Karl-Schwarzschild-StraÙe 2, 85748, Garching, Germany*

<sup>3</sup>*Mitchell Institute for Fundamental Physics & Astronomy, Department of Physics & Astronomy, Texas A&M University, College Station, TX 77843, USA*

<sup>4</sup>*State University of New York, Oswego, NY 13126, USA*

<sup>5</sup>*Graduate Institute of Astronomy, National Central University, Jhongli 32001, Taiwan*

(Received; Revised; Accepted)

ABSTRACT

We present time-series observations of Population II Cepheids in the Large Magellanic Cloud at near-infrared ( $JHK_s$ ) wavelengths. Our sample consists of 81 variables with accurate periods and optical ( $VI$ ) magnitudes from the OGLE survey, covering various subtypes of pulsators (BL Herculis, W Virginis and RV Tauri). We generate light curve templates using high-quality  $I$ -band data in the LMC from OGLE and  $K_s$ -band data in the Galactic Bulge from VVV and use them to obtain robust mean magnitudes. We derive Period-Luminosity (P-L) relations in the near-infrared and Period-Wesenheit (P-W) relations by combining optical and near-infrared data. Our P-L and P-W relations are consistent with published work when excluding long-period RV Tauris. We find that Pop II Cepheids and RR Lyraes follow the same P-L relations in the LMC. Therefore, we use trigonometric parallax from the *Gaia DR1* for VY Pyx and the *Hubble Space Telescope* parallaxes for  $k$  Pav and 5 RR Lyrae variables to obtain an absolute calibration of the Galactic  $K_s$ -band P-L relation, resulting in a distance modulus to the LMC of  $\mu_{\text{LMC}} = 18.54 \pm 0.08$  mag. We update the mean magnitudes of Pop II Cepheids in Galactic globular clusters using our light curve templates and obtain distance estimates to those systems, anchored to a precise late-type eclipsing binary distance to the LMC. We find the distances to these globular clusters based on Pop II Cepheids are consistent (within  $2\sigma$ ) with estimates based on the  $M_V - [\text{Fe}/\text{H}]$  relation for horizontal branch stars.

*Keywords:* stars: variables: Cepheids; galaxies: Magellanic Clouds, cosmology: distance scale

## 1. INTRODUCTION

Classical Cepheid variables are Population I stars used as standard candles for the extragalactic distance scale, thanks to their high luminosities and a well-defined Period-Luminosity relation (PLR) (the ‘‘Leavitt Law’’, Leavitt & Pickering 1912). They are the primary distance indicator used in the most accurate and precise determination of the Hubble constant to date (Riess et al. 2016). Type II Cepheids (hereafter, T2Cs) are low-mass, Pop II stars which can be found in globular clusters, disk, bulge and halo environments (Wallerstein 2002; Sandage & Tammann 2006). Classical and T2Cs follow different PLRs, with the latter more than a magnitude fainter than the former at similar periods. T2Cs are further classified based on their periods as BL Herculis (BLH,  $1 \lesssim P \lesssim 4$  d), W Virginis (WVI<sup>1</sup>,  $4 \lesssim P \lesssim 20$  d) and RV Tauri (RVT,  $P \gtrsim 20$  d). The classification of RVT is often ambiguous because they show irregular light curves, but they are considered a subtype of T2Cs (Sandage & Tammann 2006; Feast et al. 2008). Soszyński et al. (2008) suggested another subtype, peculiar W Virginis (PWV,  $4 \lesssim P \lesssim 10$  d), with distinct light curves that are mostly brighter and bluer than WVI.

The PLRs of T2Cs at optical bands have been studied extensively (Nemec et al. 1994; Alcock et al. 1998; Kubiak & Udalski 2003; Majaess et al. 2009; Schmidt et al. 2009, and references therein). These relations exhibit possible non-linearities, which coupled with fainter absolute magnitudes (relative to Classical Cepheids) limits their use as potential distance indicators. The third phase of the Optical Gravitational Lensing Experiment (OGLE-III) presented optical light curves and PLRs for T2Cs in the Galactic Bulge and the Magellanic Clouds (MCs) in Soszyński et al. (2008, 2010, 2011). They found that Bulge T2Cs are dominated by short-period BLH stars which are more luminous than their counterparts in the Clouds, and that LMC RVT stars lie above the PLR followed by the shorter-period classes. Theoretical studies of T2Cs based on pulsating models and evolutionary calculations by Bono et al. (1997) found that their masses decrease with increasing period and they follow a Period-Luminosity-Amplitude relation in the  $B$  band.

Over the past decade, the increased availability of large-format and higher-quality near-infrared (hereafter, NIR) detectors has made it possible to study increasingly larger samples of Cepheids at longer wavelengths where PLRs are less sensitive to extinction and metal-

licity (Madore & Freedman 1991). Matsunaga et al. (2006, 2009, 2011) derived NIR PLRs for T2Cs in Galactic globular clusters (GGCs) and the MCs. The authors found evidence for different slopes in the PLRs of each system as well as a varying frequency of each subtype. Feast et al. (2008); Groenewegen et al. (2008); Ciechanowska et al. (2010) discussed the application of NIR PLRs of T2Cs and Groenewegen et al. (2008) estimated a distance to the Galactic Center of  $R_0 = 7.94 \pm 0.37$  kpc using these variables. Recently, Ripepi et al. (2015) presented  $JK_s$  observations of T2Cs in the MCs from the VMC survey (Cioni et al. 2011) and derived a variety of P-L, Period-Luminosity-Color (PLC) and Period-Wesenheit relations (PWR).

This paper is the fourth in a series of articles based on observations obtained by the Large Magellanic Cloud Near-infrared Synoptic Survey (LMCNIS, Macri et al. 2015, hereafter, Paper I). Paper I presented survey details and the absolute calibration of NIR PLRs for Classical Cepheids. Bhardwaj et al. (2016b,a, hereafter, Papers II and III) derived PWRs for Classical Cepheids, studied possible non-linearities in the Leavitt Laws and estimated Cepheid-based distances to Local Group galaxies. In this paper we focus on the NIR observations of T2Cs and their corresponding relations.

The rest of the paper is structured as follows: §2 describes the observations, data reduction and photometry of T2Cs; §3 discusses the variation of light-curve parameters as a function of period and wavelength and the construction of templates; §4 contains the derivation of NIR PLRs and PWRs, a comparison to published work, and an estimate of the distance to the LMC; §5 presents template fits to observations of T2Cs in Galactic globular clusters and the resulting distance estimates; §6 summarizes our results.

## 2. THE DATA

Macri et al. (2015, Paper I) carried out a time-series survey of 18 sq. deg. in the central region of the LMC at  $JHK_s$  wavelengths using the 1.5-m telescope at the Cerro Tololo Interamerican Observatory and the CPA-PIR camera. Observations were carried out in queue mode by the SMARTS consortium during 32 nights from Nov 2006 to Nov 2007. The survey products include measurements for more than  $3.5 \times 10^6$  sources, including  $\sim 1500$  Classical Cepheids. Interested readers should refer to Paper I for details of the data reduction, time-series photometry, magnitude calibration and artificial star simulations used to derive crowding corrections. Given the fainter nature of T2Cs, their crowding corrections were more significant than those of Classical

<sup>1</sup> We exclusively use ‘‘WVI’’ to refer to this subtype and not to the Wesenheit relation in the  $VI$  bands.

**Table 1.** Time-series photometry for Type II Cepheids.

ID	Band	MJD	Phase	mag	$\sigma$
025	<i>J</i>	42.620	0.879	13.633	0.021
025	<i>J</i>	42.753	0.881	13.609	0.021
...	...	...	...	...	...
025	<i>H</i>	42.623	0.879	13.513	0.018
025	<i>H</i>	42.756	0.881	13.451	0.040
...	...	...	...	...	...
025	<i>K<sub>s</sub></i>	42.625	0.879	13.348	0.015
025	<i>K<sub>s</sub></i>	42.758	0.881	13.370	0.032
...	...	...	...	...	...

NOTE— ID: OGLE-LMC-T2CEP-NNN, from OGLE-III catalog of Type II Cepheids (Soszyński et al. 2008); MJD = JD − 2450000; phase is determined using the period and time of maximum brightness in *I*-band from OGLE-III. Fifth column represents magnitude in a near-infrared band and sixth column lists its associated uncertainty. The entire table is available online as supplemental material; sample time-series in *JHK<sub>s</sub>* for a T2Cs is shown here for guidance regarding its content.

Cepheids and ranged from 0.001 mag to 0.10, 0.08 and 0.27 mag in *JHK<sub>s</sub>*, respectively.

We cross-matched the LMCNISS catalog against OGLE-III (Soszyński et al. 2008) and identified 81 T2Cs with periods ranging from 1 to 68 d; 70 of these have *JHK<sub>s</sub>* measurements while the remaining 11 only have data in *J* and/or *H*-band. The sample consists of 16 BLH, 31 WVI, 12 PWV and 22 RVT stars. The NIR times-series photometry for these objects are presented in Table 1. We adopt the period (*P*), time of maximum brightness in *I*-band ( $T_{I,\max}$ ) and optical (*VI*) mean magnitudes from OGLE-III.

### 3. LIGHT CURVE ANALYSIS

We compiled multi-wavelength data available in the literature in order to study the variation in T2C light curve structure as a function of period and bandpass. The sources used were: optical photometry from OGLE-III for 203 objects in the LMC (Soszyński et al. 2008) and 357 variables in the Bulge (Soszyński et al. 2011), NIR light curves of 46 stars in Galactic globular clusters (Matsunaga et al. 2006), and *K<sub>s</sub>*-band light curves of 130 variables in the LMC (Ripepi et al. 2015). We

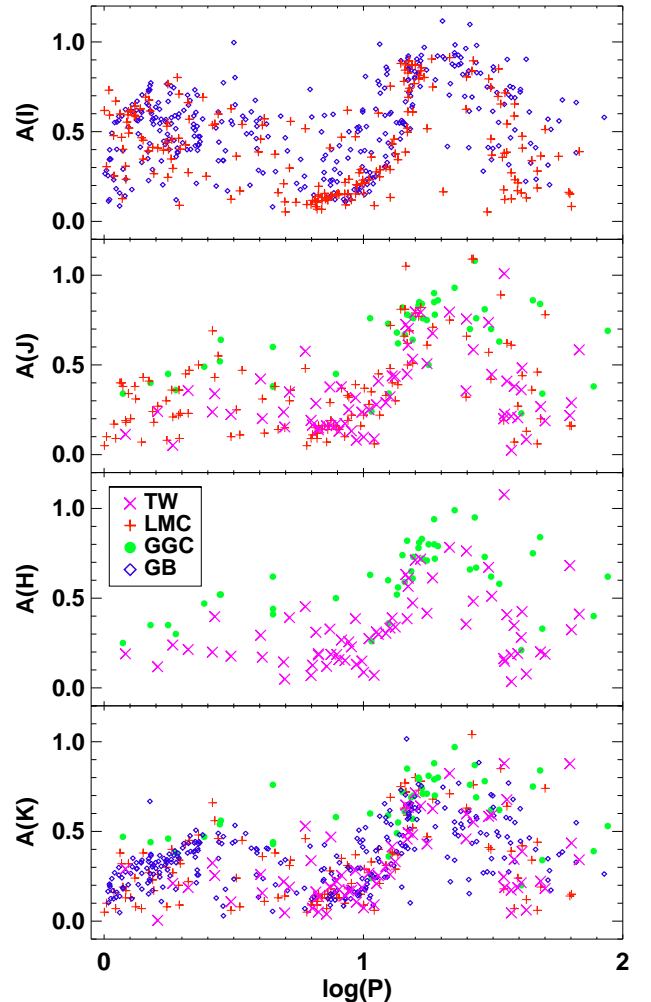


**Figure 1.** Amplitudes at various wavelengths for Type II Cepheids in the Galactic Bulge (GB, Soszyński et al. 2011; Minniti et al. 2010), Galactic globular clusters (GGC, Matsunaga et al. 2006) and the LMC (Soszyński et al. 2008; Ripepi et al. 2015). “TW” represents the amplitudes for T2Cs in the LMC based on our observations.

also cross-matched the OGLE-III catalog of Bulge T2Cs against the latest catalog (DR4, Hempel et al. , in prep.) from the VVV survey (Minniti et al. 2010). We obtained  $\sim 225$  good quality light curves with an average of 50 epochs in the *K<sub>s</sub>*-band, which were used in the analysis presented below. Details regarding the cross-match, selection criteria, photometry and other properties will be presented in a separate study (Bhardwaj et al. , in prep.).

We fit each *IJK<sub>s</sub>* light curve with a fourth-order Fourier sine series,  $m = m_0 + \sum_{i=1}^4 A_i \sin(2\pi\phi + \Phi_i)$  (Bhardwaj et al. 2015), where *m* is the observed magnitude, *A<sub>i</sub>* is the amplitude of each term and  $\phi$  rep-

resents the corresponding phase. The series is kept to  $i \leq 4$  because the number of observations is small and most light curves have large gaps in phase. Fig. 1 shows the total amplitude of each variable in each band as a function of period. We also plot the amplitudes derived by Ripepi et al. (2015) for comparison. The amplitude increases as a function of period for WVI stars with periods 8-20 d, while it exhibits the opposite behavior for RVT variables. The  $I$ -band amplitudes are the best determined since those light curves are of much higher quality. The short-period BLH stars are fainter and the long-period RVT stars exhibit irregular light curves. Therefore, the amplitudes for these variables display a greater scatter as compared to WVI stars. A more detailed discussion on variation of light curve parameters as a function of period and wavelength for (Classical) Cepheids is presented in Bhardwaj et al. (2016c).

### 3.1. Templates for Type II Cepheids

The NIR photometry of T2Cs available in the literature does not have sufficient phase coverage or photometric accuracy to construct light curve templates for these type of variables. For example, the light curves of T2Cs in the LMC currently available from the VMC survey have an average of 12 epochs in the  $K_s$ -band, while the  $J$ -band photometry is limited to only a couple of epochs (Ripepi et al. 2015). T2Cs in Galactic globular clusters have 9-40 observations per light curve but the sample is limited to 46 stars (Matsunaga et al. 2006). There are no other near-infrared time-series studies on T2Cs in the literature, thus, limiting the sample size and the phase coverage for each period range. Therefore, we use OGLE-III LMC  $I$ -band data for the purpose of constructing templates. We also use  $K_s$ -band photometry from VVV to construct an alternative set of templates for comparison. Fig. 2 displays the  $I$ -band Fourier parameters for T2Cs in the LMC and Bulge. Note that the coefficients associated with the lower order Fourier amplitudes ( $R_{21}$  and  $R_{31}$ ) and phases ( $\phi_{21}$  and  $\phi_{31}$ ) contain most of the quantitative information about light curve structure (Simon & Lee 1981; Bhardwaj et al. 2016c). The mean Fourier parameters exhibit similar variations as a function of period for both LMC and Bulge samples in the  $I$ -band. Therefore, it is reasonable to assume that the light curve structure in the  $K_s$ -band is also similar for both populations, as metallicity effects are less pronounced at longer wavelengths. The final calibrator sample consists of 170  $I$ -band and 225  $K_s$ -band light curves in the LMC and Bulge, respectively. We divide the  $I$  and  $K_s$ -band light curves into 10 period bins as the mean Fourier parameters vary significantly as a function of this parameter. The period is the best observable

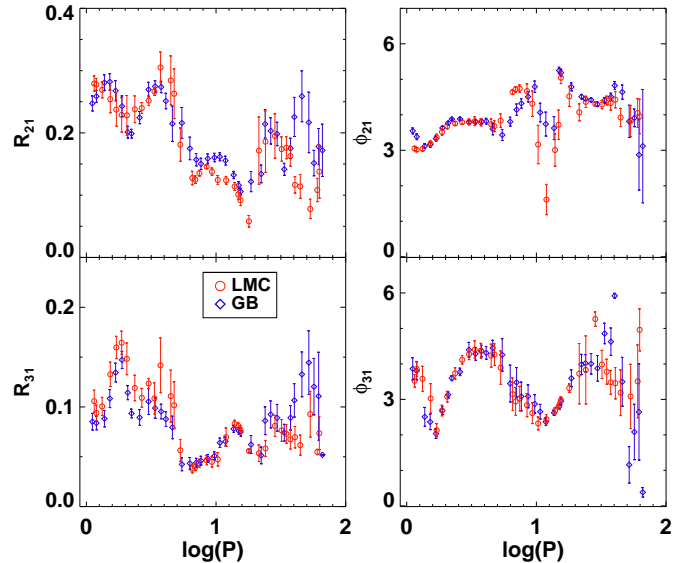


**Figure 2.** Mean Fourier parameters in  $I$ -band for Type II Cepheids in the Galactic Bulge and the LMC. The  $\phi_{31}$  parameter is converted to a cosine series for plotting purposes.

to trace the changes in light curve structure because it is independent of the wavelength. The adopted period bins and the number of stars in each bin are listed in Table 2. The number of stars per bin ranges from 8 to 69, with a significant fraction consisting of BLH stars having  $P \lesssim 2$  d. The median photometric uncertainty per bin is  $\sim 0.01$  and  $\sim 0.1$  mag for  $I$  and  $K_s$ -band, respectively.

Inno et al. (2015) recently derived near-infrared templates for Classical Cepheids and suggested that setting the zero phase of the light curves to the epoch of mean brightness would avoid problems in estimating precise maximum for bump Cepheid light curves with poor phase coverage. Although the calibrating sample of T2Cs has very good phase coverage in both  $I$  and  $K_s$ -band, we adopt the same phasing strategy to avoid any complications. We first fit light curves with a fourth-order Fourier series and determine the phase corresponding to mean magnitude along the rising branch. We normalize the light curves to zero mean and unity amplitude and merge those within an adopted period bin. We then adopt a seventh-order Fourier series as the optimum fit, following previous work on templates by Soszyński et al. (2005); Inno et al. (2015). The residuals from these fits follow a normal distribution and we recursively remove  $3\sigma$  outliers to increase the robustness of our results. The merged light curves and the Fourier series fits are displayed in Fig. 3, while the Fourier coefficients are listed in Table 3.  $T_1, T_2, \dots, T_{10}$  represent the merged light curve templates in each bin. Typical

**Table 2.** Adopted period bins

Bin	$P$ (d)	$N_I$	$N_{K_s}$
1	1-2	48	69
2	2-3	11	30
3	3-5	10	18
4	5-7	15	8
5	7-9	21	21
6	9-11	12	22
7	11-13	9	14
8	13-15	12	16
9	15-20	15	13
10	>20	17	14

NOTE— Period range for each bin is provided in second column.  $N_I$  and  $N_{K_s}$  represent the number of stars in each bin with good-quality light-curves in  $I$  and  $K_s$ -band, respectively.

standard deviations of the template fits are  $\lesssim 0.01$  mag and 0.01 in  $I$  and  $K_s$ -band, respectively. It is evident that the progression of the normalized and merged templates in each bin is similar for both bands, although the  $K_s$ -band templates are based on a significantly smaller number of data points. While the seventh-order series fits result in some wiggles for the  $K_s$ -band templates, it has no impact on the derived mean magnitudes. For example, the Fourier fits for the  $T_4$  and  $T_{10}$  sets could have been done at lower order, but we decided to retain the same expansion to facilitate the comparison with  $I$ -band templates.

#### 4. LEAVITT LAWS FOR TYPE II CEPHEIDS

We phase the NIR light curves of T2Cs in the LMC using the OGLE-III values of  $P$  and  $T_{I,\max}$  (Soszyński et al. 2008). We use the same technique described above to set the zero phase of the light curves to the time of mean light in the rising branch. We fit the templates from Table 3 and solve independently for each amplitude and a possible phase shift in the time of mean light relative to  $I$ -band. The amplitudes derived through this procedure show similar trends to those obtained via Fourier fit and no significant phase shifts are seen. Fig. 4 shows representative light curves for each T2C class. Template-fit light curves for all variables in our sample are presented in Fig. 11. We note that short-period (fainter) objects exhibit larger scatter than

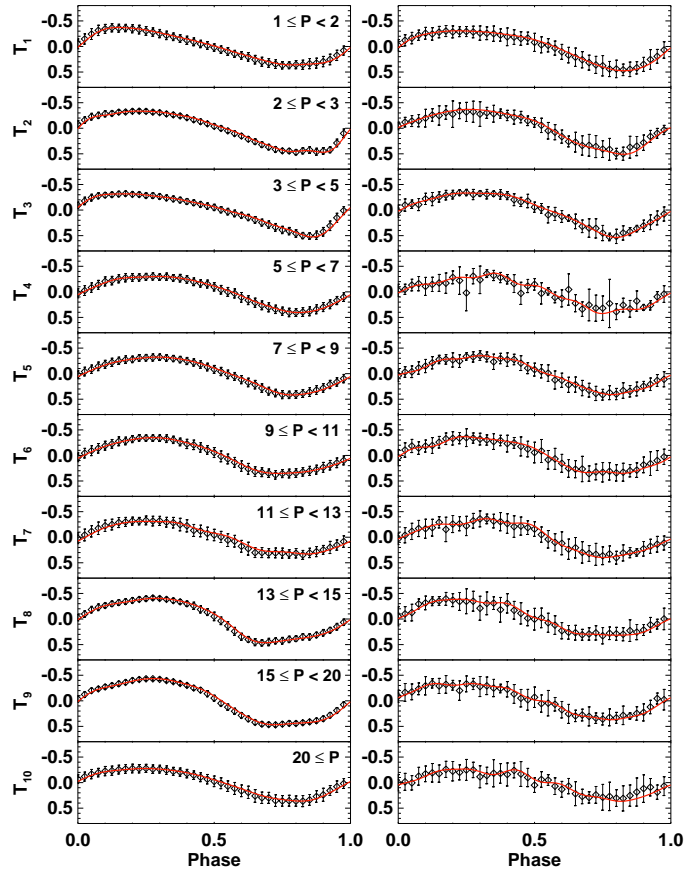


**Figure 3.** Median light curves for different period bins, based on observations of Type II Cepheids in the LMC at  $I$ -band (left) and the Galactic Bulge at  $K_s$ -band (right). The binning step size is 0.025 in phase, with the average value and standard deviation of the mean displayed with diamond symbols and error bars. The solid red lines represent seventh-order Fourier fits. The adopted range of periods (in days) for each bin, is labeled in the top right corner of the left panel.

long-period (brighter) stars, as expected from photon statistics.

The mean magnitudes are estimated via intensity-weighted integration of the best-fit  $I$  and  $K_s$ -band based templates. The standard errors on the mean magnitudes are based on the  $rms$  of the fits. The difference in the values obtained from  $I$  or  $K_s$ -band templates is  $\lesssim 0.01$  mag for  $P > 8$  d and  $\sim 0.02$  mag for shorter periods. In the case of a few BLH stars, the difference in  $K_s$ -band exceeds 0.05 mag but since the crowding corrections for most of these objects exceeds 0.2 mag, they will not be used in the final PLR fits. We take the average of both template-fit mean magnitudes as the final value. Table 4 lists the T2C mean magnitudes and uncertainties in each band. The  $JHK_s$  mean magni-

**Table 3.** Fourier coefficients of the light-curve templates for Type II Cepheids.

Bin	$A_1$	$A_2$	$A_3$	$A_4$	$A_5$	$A_6$	$A_7$	$\phi_1$	$\phi_2$	$\phi_3$	$\phi_4$	$\phi_5$	$\phi_6$	$\phi_7$	$\sigma$
<i>I</i> -band															
1	0.361	0.088	0.033	0.019	0.010	0.002	0.002	3.138	3.164	2.835	2.822	2.855	3.295	0.045	0.005
2	0.408	0.091	0.042	0.030	0.026	0.017	0.011	2.944	3.412	3.429	3.462	3.693	3.914	4.382	0.002
3	0.365	0.135	0.061	0.027	0.010	0.002	0.002	2.981	3.426	3.841	4.250	4.589	5.563	1.304	0.003
4	0.352	0.052	0.009	0.000	0.004	0.003	0.003	2.879	3.716	3.801	1.192	5.833	4.261	4.756	0.005
5	0.362	0.046	0.011	0.006	0.005	0.003	0.001	2.881	3.898	5.045	1.545	3.287	4.830	6.009	0.004
6	0.357	0.009	0.016	0.011	0.003	0.003	0.001	2.986	4.778	1.775	3.465	0.874	2.383	2.968	0.005
7	0.332	0.035	0.012	0.016	0.013	0.007	0.003	2.928	3.099	2.589	2.903	5.821	1.984	2.012	0.008
8	0.446	0.043	0.041	0.027	0.004	0.004	0.001	3.079	5.385	2.518	3.832	0.974	2.593	6.001	0.002
9	0.471	0.028	0.030	0.028	0.011	0.001	0.002	3.030	4.583	2.997	3.836	3.793	3.646	2.417	0.001
10	0.318	0.055	0.020	0.006	0.002	0.004	0.002	3.044	3.860	4.047	4.748	6.039	1.181	2.433	0.007
<i>K<sub>s</sub></i> -band															
1	0.381	0.100	0.024	0.012	0.005	0.004	0.002	2.895	3.661	3.681	3.801	3.629	3.714	3.394	0.009
2	0.421	0.071	0.015	0.025	0.012	0.005	0.002	2.957	4.093	4.509	4.984	0.043	0.622	1.530	0.008
3	0.405	0.073	0.028	0.016	0.006	0.006	0.003	2.914	4.032	4.910	0.408	3.104	2.779	3.042	0.005
4	0.351	0.043	0.018	0.023	0.012	0.024	0.021	2.895	4.366	4.554	2.869	4.454	4.199	0.961	0.013
5	0.363	0.030	0.010	0.010	0.007	0.011	0.013	2.885	4.292	4.832	0.594	4.471	5.421	4.353	0.008
6	0.362	0.026	0.017	0.028	0.007	0.013	0.011	2.958	4.837	2.379	4.467	3.568	2.370	2.487	0.013
7	0.365	0.060	0.022	0.008	0.018	0.018	0.004	2.897	4.832	2.356	3.440	1.580	5.186	2.610	0.013
8	0.371	0.020	0.028	0.004	0.016	0.011	0.012	3.091	3.158	2.789	0.581	5.449	1.873	5.638	0.013
9	0.357	0.047	0.017	0.013	0.011	0.007	0.017	3.129	3.903	3.743	2.693	5.985	1.475	5.316	0.012
10	0.297	0.051	0.009	0.023	0.019	0.020	0.017	2.874	3.766	1.938	6.167	4.367	0.966	4.343	0.017

tudes were corrected for extinction using the reddening law of [Cardelli et al. \(1989\)](#) with  $R_V = 3.23$  and individual reddening values from the map of [Haschke et al. \(2011\)](#). The total-to-selective absorption ratios per unit of  $E(V - I)$  are  $R_J = 0.69$ ,  $R_H = 0.43$  and  $R_K = 0.28$  ([Bhardwaj et al. 2016b](#)).

We fit PLRs of the following form:

$$m_\lambda = a_\lambda[\log(P) - 1] + b_\lambda, \quad (1)$$

where  $m_\lambda$  is the extinction-corrected mean magnitude,  $\lambda$  represents the  $JHK_s$  bands,  $a$  is the slope and  $b$  is the zeropoint at  $P = 10$  d. We fit PLRs to the entire sample as well as to subsamples of faint (BLH+WVI) and bright (PWV+RVT) variables, iteratively removing  $2\sigma$  outliers in all cases. As most of the outliers are likely due to blends or additional crowding effects, they appear on the bright side of the PLRs (see also discussion in [Matsunaga et al. 2009](#); [Ripepi et al. 2015](#)). We adopt

this threshold throughout the paper to have a stronger constraint on slopes and zeropoints. Since the samples are small, a higher sigma-clipping threshold marginally changes the slopes (by less than the half of their quoted uncertainties) and the typical increase in the number of stars and the dispersion is less than 10%. Fig. 5 displays the results of the fits, which are also summarized in Table 5. We also note that a detailed statistical analysis on P-L relations was presented in Paper III to test Classical Cepheid data for non-linearity under various assumptions such as independent identically distributed observations, normality of residuals and homoskedasticity. We also performed White’s test ([White 1980](#)) for Type II Cepheid sample and found that our data provide evidence of homoskedasticity under 95% confidence interval.

Previous studies at optical and NIR wavelengths (see, [Soszyński et al. 2008](#); [Matsunaga et al. 2009](#);

**Table 4.** Properties of Type II Cepheids in the LMC.

ID	P (d)	Class	Mean magnitudes					$\sigma$			$E(V - I)$ [mag]
			$V$	$I$	$J$	$H$	$K_s$	$J$	$H$	$K_s$	
OGLE-LMC-T2CEP-025	67.965	RVT	15.102	14.042	13.554	13.209	13.160	0.059	0.084	0.120	0.070
OGLE-LMC-T2CEP-028	8.785	PWV	16.045	15.543	15.340	14.881	14.732	0.056	0.045	0.072	0.050
OGLE-LMC-T2CEP-029	31.245	RVT	15.446	14.642	14.020	13.607	13.354	0.028	0.040	0.041	0.040
OGLE-LMC-T2CEP-033	9.395	PWV	16.468	15.788	15.253	14.887	14.845	0.044	0.055	0.054	0.050
OGLE-LMC-T2CEP-034	14.911	WVI	17.317	16.228	15.485	14.971	14.797	0.057	0.054	0.048	0.080
OGLE-LMC-T2CEP-035	9.866	WVI	17.162	16.259	15.637	15.127	15.048	0.050	0.054	0.078	0.050
OGLE-LMC-T2CEP-036	14.881	WVI	16.745	15.845	15.161	14.692	14.634	0.036	0.053	0.059	0.050

NOTE—Star ID, period, class and mean  $VI$  magnitudes are taken from OGLE-III [Soszyński et al. \(2008\)](#).  $E(V - I)$  values are based on the maps of [Haschke et al. \(2011\)](#). The entire table is available online as supplemental material; only a few lines are shown here for guidance regarding its content.

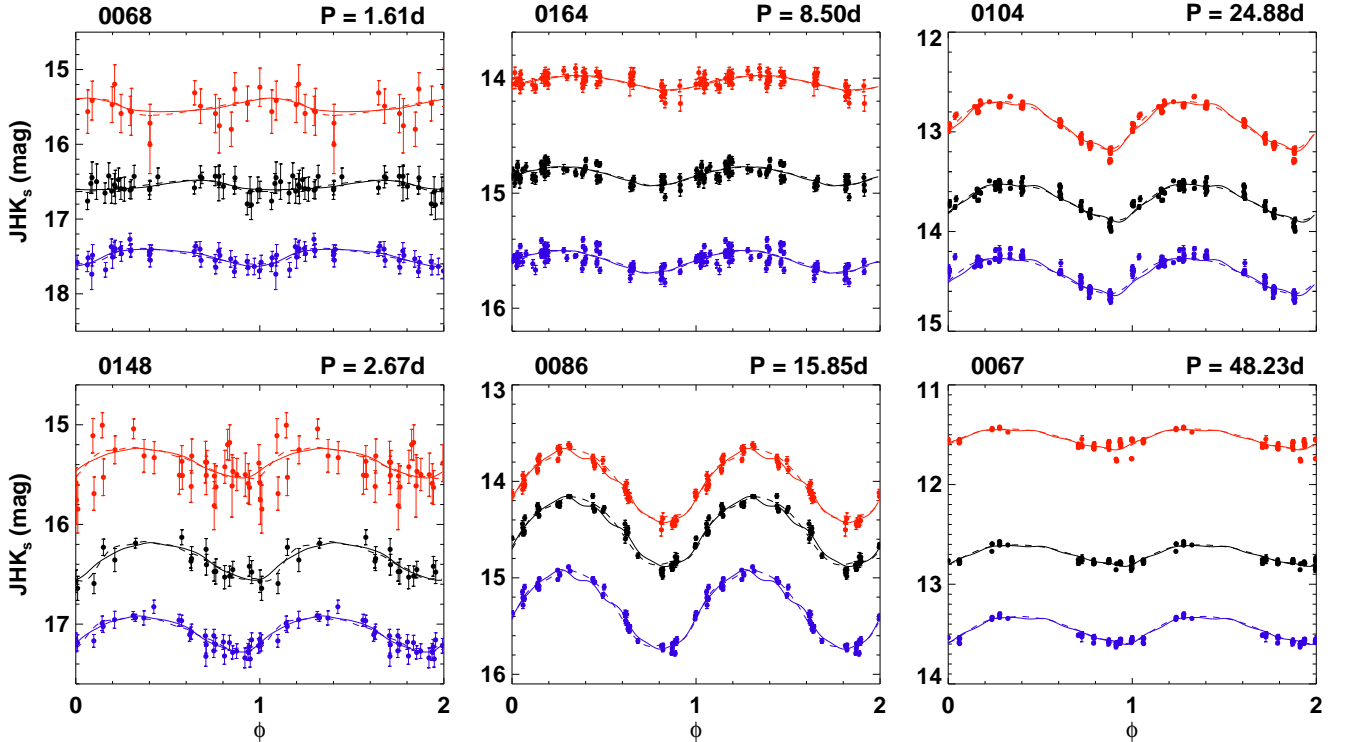


**Figure 4.** Representative near-infrared light curves of six Type II Cepheids in the LMC. The left, middle and right panels show short, intermediate and long-period BLH, WVI and RVT stars, respectively.  $J$ ,  $H$  and  $K_s$ -band light curves are plotted using blue, black and red symbols. The  $J$  and  $K_s$ -band light curves are offset by  $+0.25$  and  $-0.5$  mag, respectively. The solid and dashed lines represent the  $I$  and  $K_s$ -band templates, respectively, fit to the data in each band.

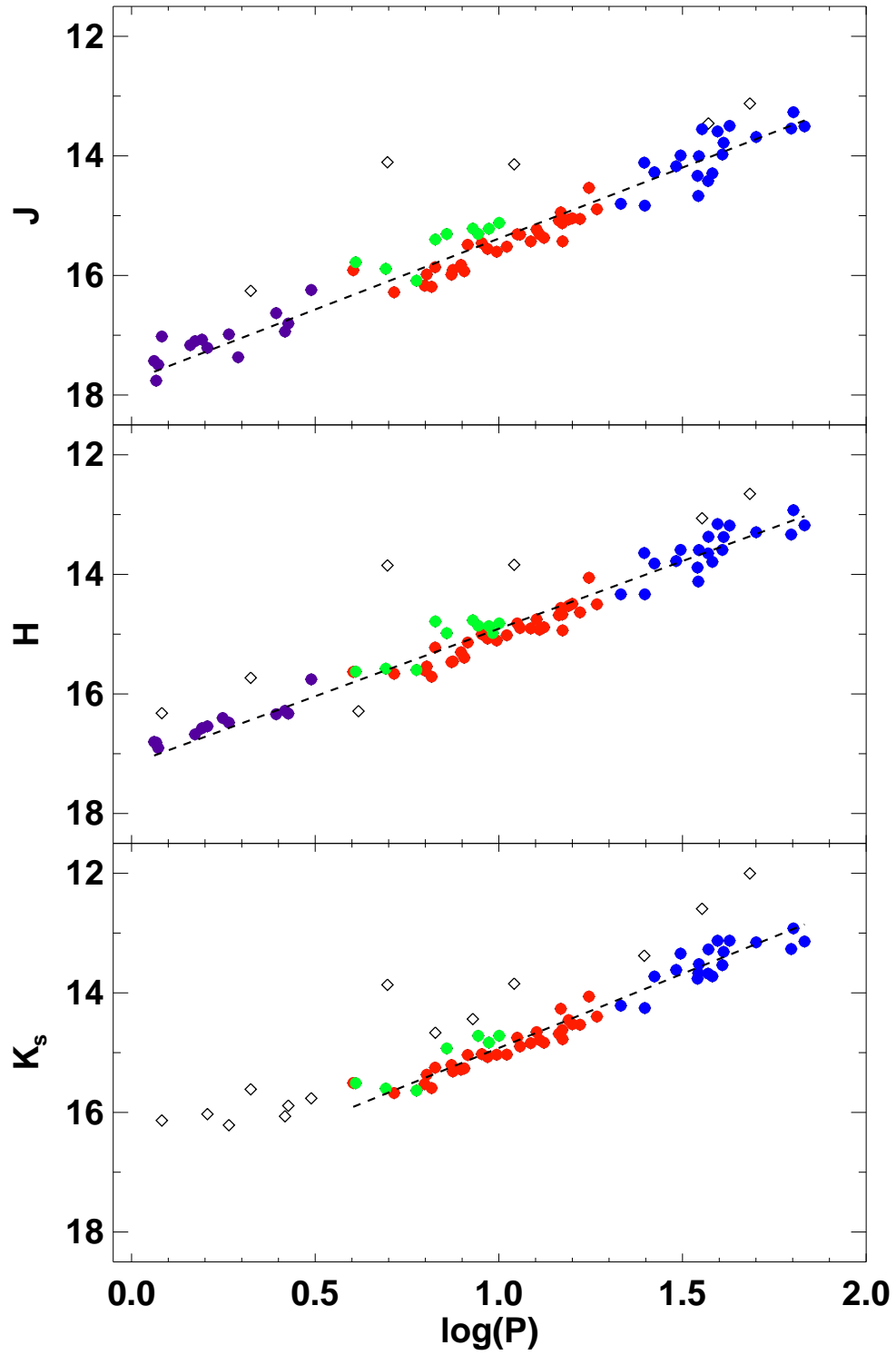


**Figure 5.** Extinction-corrected near-infrared P-L relations for Type II Cepheids in the LMC, based exclusively on our photometry. The violet, red, green and blue symbols represent BLH, WVI, PWV and RVT stars, respectively. The dashed line represents a single regression line over the entire period range and open diamonds show  $2\sigma$  outliers.



**Table 5.** Type II Cepheid P-L Relations in the LMC based exclusively on our photometry.

Band	Types	$a$	$\sigma_a$	$b$	$\sigma_b$	$rms$	$N$
$J$	B+W	-2.100	0.107	15.539	0.038	0.149	40
$J$	P+R	-2.256	0.111	15.168	0.059	0.274	30
$J$	all	-2.374	0.058	15.383	0.026	0.259	73
$H$	B+W	-1.963	0.109	15.053	0.042	0.110	39
$H$	P+R	-2.188	0.116	14.767	0.060	0.239	31
$H$	all	-2.261	0.061	14.908	0.028	0.208	72
$K_s$	B+W	-2.117	0.318	14.992	0.047	0.081	26
$K_s$	P+R	-2.062	0.118	14.627	0.063	0.244	29
$K_s$	all	-2.483	0.089	14.922	0.038	0.190	56

NOTE—B+W: BLH+WVI; P+R: PWI+RVT.

**Table 6.** Comparison of Type II Cepheid P-L relations.

Band	$a$	$\sigma_a$	$rms$	$N$	Loc	Src	$ T $	$p(t)$
$J$	-2.374	0.058	0.259	73	LMC	TW	...	...
$J$	-2.163	0.044	0.210	137	LMC	M09	3.017	0.003
$J$	-2.190	0.040	0.130	120	LMC	R14	2.557	0.011
$J$	-2.092	0.116	0.330	47	SMC	M11	2.344	0.021
$J$	-2.230	0.053	0.160	46	GGC	M06	1.591	0.114
$H$	-2.261	0.061	0.208	72	LMC	TW	...	...
$H$	-2.316	0.043	0.200	136	LMC	M09	0.746	0.457
$H$	-2.214	0.148	0.320	25	SMC	M11	0.357	0.722
$H$	-2.344	0.050	0.150	46	GGC	M06	0.996	0.321
$K_s$	-2.483	0.089	0.190	56	LMC	TW	...	...
$K_s$	-2.278	0.047	0.210	129	LMC	M09	1.933	0.055
$K_s$	-2.385	0.030	0.090	120	LMC	R14	1.312	0.191
$K_s$	-2.113	0.105	0.290	45	SMC	M11	2.609	0.011
$K_s$	-2.408	0.047	0.140	46	GGC	M06	0.768	0.444
$K_s$	-2.240	0.140	0.410	39	GB	G08	1.399	0.165

NOTE—Loc: LMC/SMC: Large/Small Magellanic Cloud, GGC: Galactic globular clusters; GB: Galactic Bulge. Src: TW: this work; M06: Matsunaga et al. (2006); G08: Groenewegen et al. (2008); M09: Matsunaga et al. (2009); M11: Matsunaga et al. (2011); R15: Ripepi et al. (2015).  $|T|$  represents the observed value of the t-statistic and  $p(t)$  gives the probability of acceptance of the null hypothesis (equal slopes).

Ripepi et al. 2015) have suggested that PWV and RVT stars lie above the PLR defined by the shorter-period BLH and WVI stars. A single PLR fit to our entire sample also gives evidence that WVI stars are mostly found below the regression line, specially in  $J$ -band. We use the  $F$ -test as described in Paper III, to quantify the statistical significance of non-linearities in the slopes of the PLRs for various subsamples. We find a considerable difference between the PLR slopes for RVTs and BLH+WVI variables when considered separately. However, we find consistent slopes between PWV+RVT stars and BLH+WVI variables. Table 5 summarizes our findings. We note that the PLR dispersions are reduced by 12%, 2% and 3% in  $JHK_s$ , respectively, when using template-fit instead of Fourier-fit magnitudes.

#### 4.1. Comparison with published $P$ - $L$ relations

We compare our PLRs to previous work carried out by Matsunaga et al. (2006), Groenewegen et al. (2008), Matsunaga et al. (2009), Matsunaga et al. (2011), and Ripepi et al. (2015). We use the t-test as discussed in Paper II, to compare the slopes given their uncertainties and the dispersion of the underlying relations. The observed t-statistic is compared with theoretical values, calculated from the t-distribution at the 95% confidence interval (see Paper II for details). In brief, the null hypothesis that the two slopes are the same is rejected if the observed t-statistic ( $|T|$ ) is greater than the theoretical ( $t$ ) value. Table 6 lists the various slopes and the results of the test-statistic. The probability ( $p(t)$ ) of the acceptance of null hypothesis is also provided and  $p(t) < 0.05$  suggests that the two slopes under consideration are not equal.

We find that the slope of the  $J$ -band PLR for our entire sample is not consistent with those derived by Matsunaga et al. (2009); Ripepi et al. (2015) for T2Cs in the LMC but it is consistent in  $H$  and  $K_s$ -bands. We note that those studies did not consider RVTs since they were found to lie well above the single regression line relative to shorter-period T2Cs at optical wavelengths. This deviation is not significant in our sample in  $K_s$ -band. The slope of the  $J$ -band PLR for BLH+WVI stars is  $-2.100 \pm 0.107$ , consistent with published work given the uncertainties. The slopes of the LMC PLRs are not consistent with their SMC counterparts in  $J$  and  $K_s$ -bands from Matsunaga et al. (2011) but are in agreement in all bands with those from globular clusters (Matsunaga et al. 2009). Furthermore, the slope of the LMC  $K_s$ -band PLR is also consistent with the corresponding relation based on Bulge variables (Groenewegen et al. 2008).

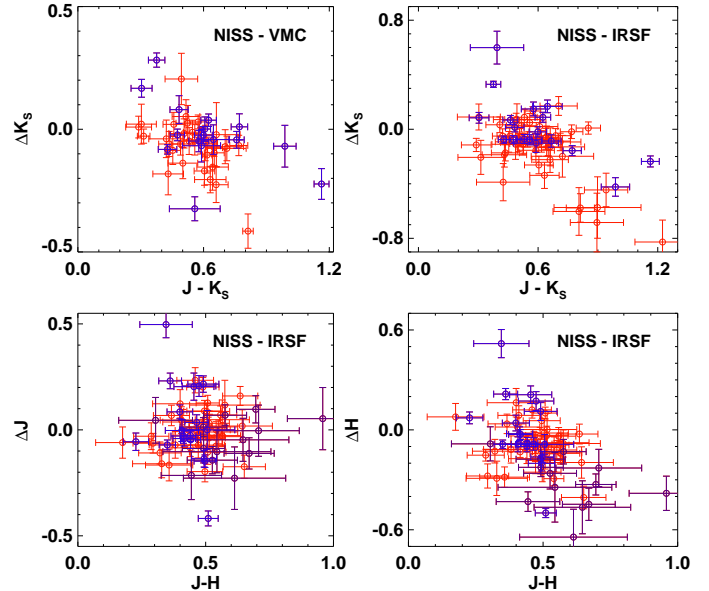


**Figure 6.** *Top left:* Comparison of  $K_s$ -band mean magnitudes as a function of  $J - K_s$  for stars in common with Ripepi et al. (2015). *Top right:* Same as top-left panel but with random-phase corrected mean magnitudes from Matsunaga et al. (2009). *Bottom panels:* Same as top-right panel but for  $J$  and  $H$ -band magnitudes as a function of  $J - H$ .

We also compare our T2C NIR mean magnitudes with values found in the literature. We find 76 objects in common with Matsunaga et al. (2011) and 62 with (Ripepi et al. 2015). We note that the former are single-epoch  $JHK_s$  measurements in the IRSF (Kato et al. 2007) system while the latter are mean magnitudes in the VISTA system. We apply the relevant color transformations from IRSF to 2MASS following (Kato et al. 2007) and from VISTA to 2MASS as derived by Cambridge Astronomy Survey Unit (2016). Fig. 6 shows the difference in our magnitudes with respect to VISTA and IRSF as a function of color. The  $K_s$ -band mean magnitudes in this work are consistent with those from VISTA given their uncertainties. The agreement with IRSF is also good except for a few stars with  $J - K_s > 0.7$  mag. The  $J$ -band magnitudes from our work and IRSF are in good agreement, while a mild trend is seen in  $H$ -band.

#### 4.2. Near-infrared $P$ - $L$ and $P$ - $W$ relations for OGLE-III sample of Type II Cepheids

We compile  $JHK_s$  magnitudes for T2Cs in the LMC that also have  $VI$  mean magnitudes from OGLE-III. We give preference to our NIR measurements, except for BLH stars in  $K_s$ -band. If measurements are not available in our database, we use  $JK_s$  mean mag-

**Table 7.** Near-infrared P-L and P-W relations for Type II Cepheids in the LMC, based on mixed photometry.

Band	Type	$a$	$\sigma_a$	$b$	$\sigma_b$	$rms$	$N$
$J$	BLH	-2.294	0.153	15.375	0.113	0.202	55
	WVI	-2.378	0.105	15.580	0.018	0.111	72
	B+W	-2.061	0.038	15.563	0.017	0.157	126
	P+R	-2.249	0.072	15.144	0.039	0.320	53
	all	-2.346	0.025	15.416	0.012	0.252	180
$H$	BLH	-2.088	0.214	15.218	0.163	0.296	52
	WVI	-2.457	0.111	15.160	0.018	0.123	72
	B+W	-2.202	0.046	15.142	0.017	0.171	117
	P+R	-2.297	0.071	14.752	0.038	0.269	52
	all	-2.484	0.029	15.034	0.013	0.241	174
$K_s$	BLH	-2.083	0.154	15.162	0.114	0.262	47
	WVI	-2.250	0.097	15.078	0.016	0.119	72
	B+W	-2.232	0.037	15.070	0.015	0.180	119
	P+R	-2.173	0.071	14.654	0.036	0.309	51
	all	-2.395	0.027	14.981	0.012	0.228	167
$W_{J,H}$	B+W	-2.437	0.071	14.455	0.029	0.328	119
	P+R	-2.174	0.112	14.095	0.061	0.337	53
	all	-2.548	0.046	14.391	0.021	0.338	172
$W_{J,K_s}$	B+W	-2.346	0.051	14.724	0.021	0.216	119
	P+R	-2.216	0.088	14.349	0.046	0.345	50
	all	-2.529	0.034	14.648	0.015	0.249	166
$W_{H,K_s}$	B+W	-2.248	0.085	14.959	0.030	0.321	115
	P+R	-2.155	0.127	14.576	0.064	0.304	45
	all	-2.478	0.057	14.832	0.023	0.369	165
$W_{V,J}$	B+W	-2.269	0.038	14.957	0.018	0.207	130
	P+R	-2.292	0.074	14.593	0.040	0.303	53
	all	-2.486	0.025	14.845	0.012	0.264	184
$W_{V,H}$	B+W	-2.328	0.044	14.724	0.017	0.221	125
	P+R	-2.388	0.072	14.442	0.039	0.268	52
	all	-2.547	0.028	14.620	0.013	0.266	180
$W_{V,K_s}$	B+W	-2.281	0.036	14.803	0.016	0.245	124
	P+R	-2.162	0.071	14.407	0.036	0.302	50
	all	-2.456	0.025	14.689	0.012	0.308	179
$W_{I,J}$	B+W	-2.267	0.045	15.003	0.020	0.189	123
	P+R	-2.277	0.083	14.588	0.045	0.315	52
	all	-2.474	0.029	14.866	0.014	0.287	182
$W_{I,H}$	B+W	-2.351	0.048	14.709	0.018	0.215	119
	P+R	-2.228	0.070	14.356	0.037	0.289	52
	all	-2.503	0.031	14.631	0.013	0.239	169
$W_{I,K_s}$	B+W	-2.342	0.039	14.797	0.016	0.180	115
	P+R	-2.148	0.071	14.392	0.036	0.312	50
	all	-2.486	0.027	14.726	0.012	0.244	167

NOTE—B+W: BLH+WVI; P+R: PWI+RVT.

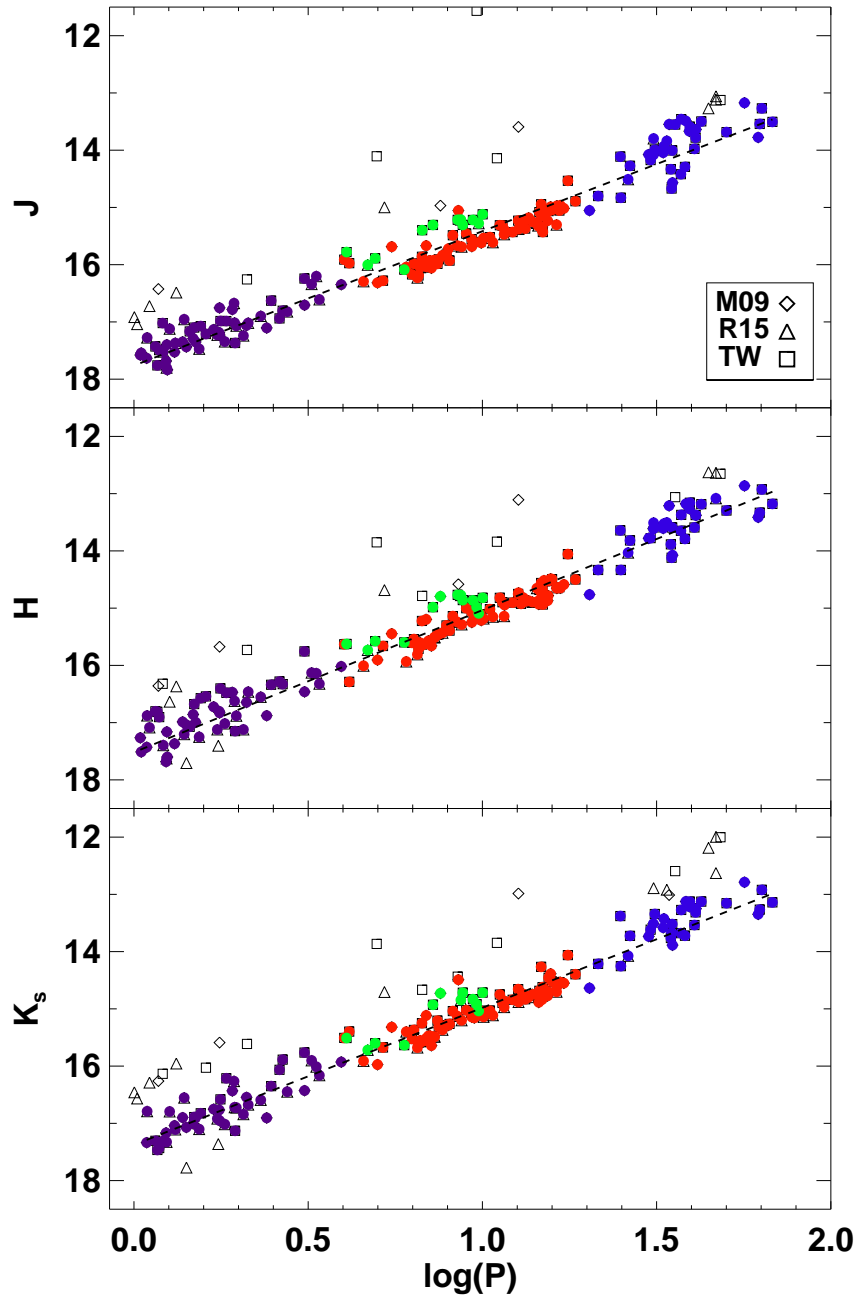


**Figure 7.** Extinction-corrected near-infrared P-L relations for OGLE-III Type II Cepheids in the LMC with photometry from our work and the literature. The violet, red, green and blue colors represent BLH, WVI, PWV and RVT stars, respectively. The square, triangle, and diamond symbols represent the photometry from this work (TW), Ripepi et al. (R15, 2015) and Matsunaga et al. (M09, 2009), respectively. The dashed line represents a single regression line over the entire period range and empty symbols show  $2\sigma$  outliers.

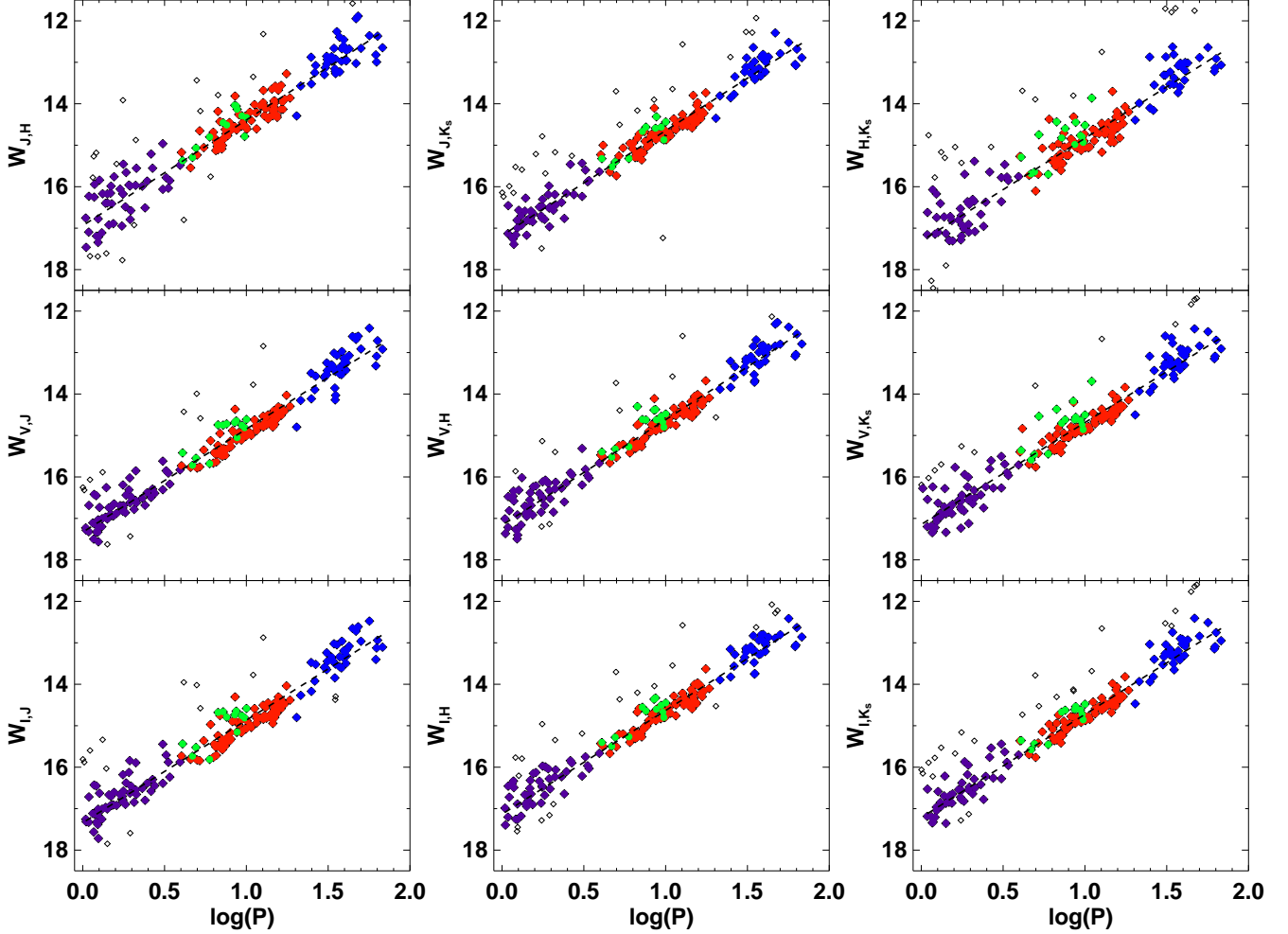


**Figure 8.** Near-infrared Period-Wesenheit relations for Type II Cepheids in the LMC. The violet, red, green and blue symbols represent BLH, WVI, PWV and RVT stars, respectively. The dashed line represents a single regression line over the entire period range and open diamonds show  $2\sigma$  outliers.

nitudes from [Ripepi et al. \(2015\)](#) or phase-corrected single-epoch magnitudes from [Matsunaga et al. \(2011\)](#) as the lowest-priority source. We thus obtain NIR magnitudes in at least one band for 197 out of the 203 OGLE T2Cs in the LMC. All measurements are transformed into the 2MASS system. We derive PLRs for each class of variable following Eqn. 1 as well as relations based on “Wesenheit” ([Madore 1982](#)) magnitudes:

$$W_{\lambda_2, \lambda_1} = m_{\lambda_1} - R_{\lambda_1}^{\lambda_2} (m_{\lambda_2} - m_{\lambda_1}), \quad (2)$$

$$R_{\lambda_1}^{\lambda_2} = \left[ \frac{A_{\lambda_1}}{E(m_{\lambda_2} - m_{\lambda_1})} \right]$$

where  $m_{\lambda}$  is the mean magnitude in one of  $VIJHK_s$  and  $\lambda_1 > \lambda_2$ . We use the [Cardelli et al. \(1989\)](#) reddening law and assume a value of total-to-selective absorption of  $R_V = 3.23$ . The resulting absorption ratios in other bands are:  $R_H^J = 1.63$ ,  $R_{K_s}^J = 0.69$ ,  $R_{K_s}^H = 1.92$ ,  $R_J^V =$

$0.41$ ,  $R_H^V = 0.22$ ,  $R_{K_s}^V = 0.13$ ,  $R_J^I = 0.92$ ,  $R_H^I = 0.42$ ,  $R_{K_s}^I = 0.24$  (see Paper II). The Wesenheit magnitudes are fit with  $\log(P)$  as an independent variable. The resulting PLRs and PWRs are plotted in Figs. 7 and 8, respectively, and summarized in Table 7.

The PWRs formed as a combination of  $I$ -band and one of  $J$ ,  $H$  or  $K_s$ -band exhibit a smaller dispersion than other NIR relations. Similarly,  $W_{J,K_s}$  displays a significantly smaller dispersion than  $W_{J,H}$  and  $W_{H,K_s}$ , presumably due to the dominant sample of template-fit mean magnitudes in  $J$  and  $K_s$ -band instead of the phase-corrected single-epoch magnitudes in  $H$ -band. We compare the PWR slopes with those of [Ripepi et al. \(2015\)](#) and find a consistent value for  $W_{V,K_s}$ , while our value for  $W_{V,J}$  is marginally steeper. However, we note that the [Ripepi et al. \(2015\)](#) results are based on a single regression fit to BLH+WVI vari-

**Table 8.** Type II Cepheids and RR Lyrae with parallaxes and pulsation distances.

ID	Type	$\log P$	$K_s$	$E_{BV}$	$\pi$	$LKH$	[Fe/H]	$\sigma_{[Fe/H]}$	Src
		[d]	[mag]		[mas]	[mag]	[dex]		
VY Pyx	BLH	0.093	5.72	0.05	$3.85 \pm 0.28$	-0.01	-0.01	0.15	<i>Gaia</i>
SW Tau	BLH	0.200	7.95	0.28	$1.37 \pm 0.04$	...	0.22	...	B-W
V553 Cen	BLH	0.314	6.86	0.00	$1.85 \pm 0.05$	...	0.24	...	B-W
<i>k</i> Pav	WVI	0.958	2.78	0.02	$5.57 \pm 0.28$	-0.02	0.00	0.13	<i>HST</i>
XZ Cyg	RRab	-0.331	8.72	0.10	$1.67 \pm 0.17$	-0.09	-1.44	0.20	<i>HST</i>
UV Oct	RRab	-0.266	8.30	0.09	$1.71 \pm 0.10$	-0.03	-1.74	0.11	<i>HST</i>
RR Lyr	RRab	-0.247	6.49	0.03	$3.77 \pm 0.13$	-0.02	-1.39	0.13	<i>HST</i>
SU Dra	RRab	-0.180	8.62	0.01	$1.42 \pm 0.16$	-0.11	-1.80	0.20	<i>HST</i>
RZ Cep	RRc	-0.511	7.88	0.08	$2.54 \pm 0.19$	-0.05	-1.77	0.20	<i>HST</i>

NOTE— $E_{BV} = E(B-V)$ . B-W distances from Feast et al. (2008) are converted to parallaxes for relative comparison.

ables and those are consistent with our results for the same subsample.

#### 4.3. Distance to the LMC using *HST* parallaxes

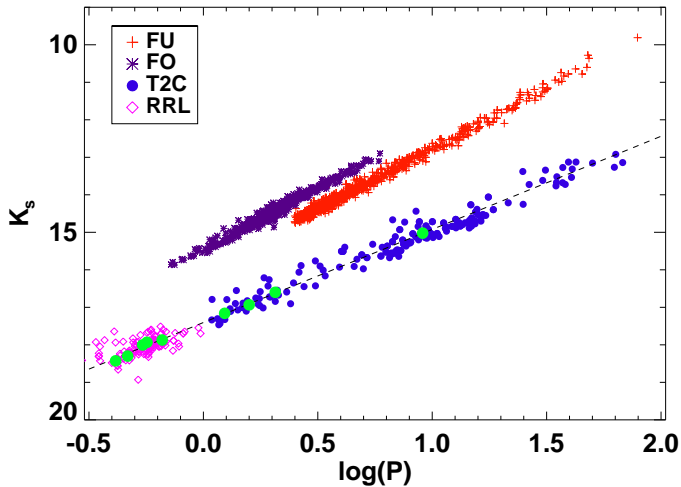


**Figure 9.** A comparison of  $K_s$ -band P-L relation with Classical Cepheids from LMCNISS data and RR Lyraes in the LMC. The green circles represent the calibrator T2Cs and RRLs.

The short-period T2Cs reside in the same instability strip that extends a few magnitudes above the horizontal branch and includes RR Lyraes (RRLs; Sandage & Tammann 2006). It has been suggested that RRLs follow the same PLRs as short period T2Cs (Sollima et al. 2006; Feast et al. 2008; Ripepi et al.

**Table 9.** Estimates of the LMC distance modulus

Source	$\mu$ [mag]
T2C $\pi$	$18.54 \pm 0.11$
RRL $\pi$	$18.55 \pm 0.10$
T2C B-W	$18.41 \pm 0.09$

2015). We therefore further extend the expanded PLRs of §4.2 with NIR measurements of RRLs in the LMC from Borissova et al. (2009); Muraveva et al. (2015), as shown in Fig. 9. It can be seen that RRLs nicely follow the PLR of T2Cs, which is shallower than those obeyed by Classical Cepheids.

We use trigonometric parallaxes for 2 T2Cs and 5 RRLs in the solar neighborhood, obtained with the *Hubble Space Telescope* (*HST*, Benedict et al. 2011) and *Gaia* (Lindegren et al. 2016), to calibrate the zeropoint of our PLRs and estimate a distance to the LMC. We also use distance estimates for two T2Cs (V553 Cen and SW Tau) determined via the Baade-Wesselink (B-W) method (Feast et al. 2008). Table 8 summarizes the distance estimates for all calibrators along with magnitudes and other properties adopted from Feast et al. (2008); Benedict et al. (2011). We include the  $LKH$  correction (Lutz & Kelker 1973) and “fundamentalize” the period of first-overtone RRL by adding  $\Delta \log(P) = 0.127$ . Lastly, RRL magnitudes are corrected for metallicity effects using the recent  $P - L_{K_s} - [Fe/H]$  relation of Muraveva et al. (2015).

$k$  Pav was classified as a PWV by Feast et al. (2008), but Benedict et al. (2011) showed that it follows the same PLR as RRLs. The *HST* and *Hipparcos* parallaxes of VY Pyx are very dissimilar ( $6.44 \pm 0.23$  mas and  $5.01 \pm 0.44$  mas from Benedict et al. 2011; van Leeuwen 2007, respectively) and yield absolute magnitudes well below the RRL PLR regression line. In contrast, the recent *Gaia* parallax ( $3.85 \pm 0.28$  mas, Lindegren et al. 2016) is in excellent agreement with expectations and is therefore used in our analysis. We note that Benedict et al. (2011) provided two parallaxes for the RRL RZ Cep; we adopt  $\pi = 2.54 \pm 0.19$  mas since the other choice makes it an outlier in the PLR.

We fix the slope of the  $K_s$ -band PLR to the value derived from our LMC photometry (“all” in Table 5) and solve for the difference between the intercept of the Galactic and LMC relations which have absolute and apparent magnitudes, respectively. We thus obtain three estimates of the distance modulus of the LMC based the weighted averages of: (1) the parallaxes of two T2Cs, (2) the parallaxes of five RRLs, and the B-W distances of two T2Cs. The results, listed in Table 9, are in good agreement with the estimates based on late-type eclipsing binaries ( $18.493 \pm 0.048$  mag, Pietrzyński et al. 2013). These values are also consistent with recent studies (Monson et al. 2012; de Grijs et al. 2014) and the estimate of  $18.47 \pm 0.07$  mag by Bhardwaj et al. (2016b) using the photometry of Classical Cepheids from Paper I. The error budget includes estimates of uncertainties due to: (1) photometry and extinction corrections (0.05 mag); (2) metallicity corrections, given the uncertainties in  $[\text{Fe}/\text{H}]$  from Benedict et al. (2011) and the metallicity correction coefficient uncertainty of 0.07 mag/dex from Muraveva et al. (2015); (3) parallaxes; (4) slope and zeropoint of PLRs. The overall uncertainties are constrained by the inverse weighted variance of the calibrators and the standard deviation of the mean added in quadrature. We note that the LMC distance modulus based on B-W distances is smaller than those based on trigonometric parallaxes, similar to the results of Feast et al. (2008). Therefore, we calculate a mean distance modulus to the LMC based only on the two independent calibrations that rely on parallaxes:  $\mu = 18.54 \pm 0.08$  mag.

## 5. DISTANCES TO GALACTIC GLOBULAR CLUSTERS

Matsunaga et al. (2006) published NIR light curves for T2Cs in 26 Galactic globular clusters and derived the corresponding PLRs. However, the definition of mean magnitude adopted by the authors was a simple mean of maximum and minimum values, which may bias

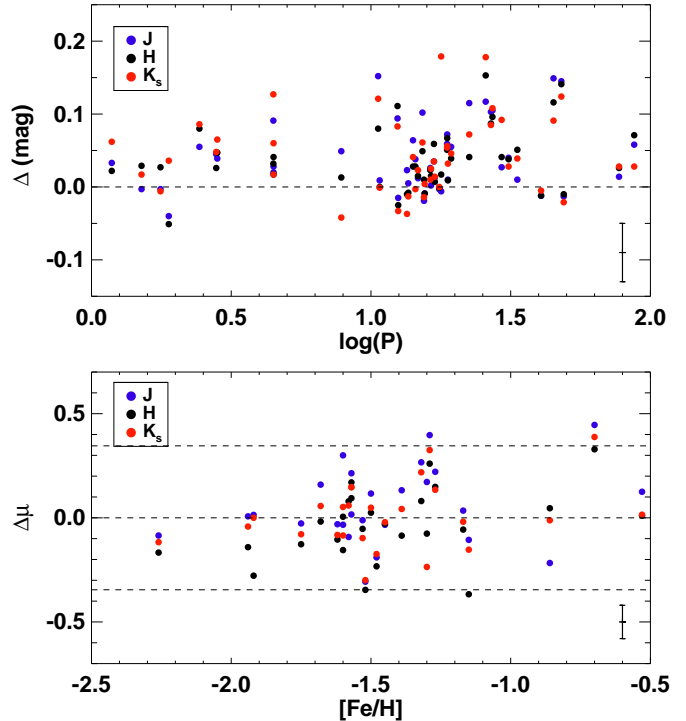


**Figure 10.** Top: difference in mean magnitudes between Matsunaga et al. (2006) and template-fit values derived in this work. Bottom: difference in distance modulus obtained by Matsunaga et al. (2006) (using the  $M_V$ - $[\text{Fe}/\text{H}]$  relation) and this work (using type II Cepheid PLRs). Dashed lines indicate  $\pm 2\sigma$  of the average difference. Representative median error bar is also displayed in each panel.

the results since the light curves are neither sinusoidal nor fairly well sampled. Therefore, we use our templates to fit their data and obtain robust mean magnitudes. The resulting light curves are displayed in Fig. 12, while the mean magnitudes are listed in Table 10. Fig. 10 displays the difference in mean magnitudes obtained via these two approaches, showing that the results from Matsunaga et al. (2006) were significantly biased towards larger values.

In order to obtain distance estimates to these globular clusters, we perform an absolute calibration of the LMC PLRs using the distance modulus derived by Pietrzyński et al. (2013) using late-type eclipsing binaries,  $\mu = 18.493 \pm 0.048$  mag. This estimate is significantly more precise and accurate than the one we obtained in § 4.3 using a few trigonometric parallaxes and was also adopted in Papers I and II to calibrate the Classical Cepheid PLRs and PWRs.

We correct the Galactic globular cluster photometry for interstellar extinction using the tabulated  $E(B - V)$  values and the Cardelli et al. (1989) extinction law. We

**Table 10.** Template-fit mean magnitudes for Type II Cepheids in Galactic globular clusters.

Cluster	Star	P	$\langle J \rangle$	$\langle H \rangle$	$\langle K_s \rangle$	$\sigma$	$E_{BV}$	[Fe/H]		
NGC 1904	V8	77.200	10.346	9.814	9.652	0.064	0.060	0.058	0.01	-1.57
NGC 2808	V10	1.765	13.893	13.513	13.436	0.039	0.033	0.044	0.22	-1.15
NGC 5139	V1	29.348	9.373	9.009	8.898	0.052	0.056	0.026	0.12	-1.60
NGC 5139	V29	14.734	10.418	10.015	9.907	0.063	0.066	0.092	0.12	-1.60
NGC 5139	V48	4.474	11.499	11.108	11.023	0.038	0.022	0.075	0.12	-1.60
NGC 5272	V154	15.284	11.348	11.011	10.929	0.044	0.037	0.034	0.01	-1.57
NGC 5904	V42	25.738	10.043	9.697	9.642	0.062	0.072	0.077	0.03	-1.27
NGC 5904	V84	26.870	10.097	9.713	9.625	0.107	0.092	0.093	0.03	-1.27
NGC 5986	V13	40.620	10.912	10.232	10.075	0.024	0.014	0.017	0.28	-1.58
NGC 6093	V1	16.304	11.624	11.207	11.090	0.039	0.050	0.038	0.18	-1.75
NGC 6218	V1	15.480	10.259	9.780	9.654	0.056	0.027	0.051	0.19	-1.48
NGC 6254	V1	48.950	9.083	8.430	8.251	0.049	0.026	0.013	0.28	-1.52
NGC 6254	V2	18.723	9.991	9.559	9.416	0.055	0.061	0.059	0.28	-1.52
NGC 6254	V3	7.831	10.971	10.537	10.402	0.045	0.020	0.074	0.28	-1.52
NGC 6256	V1	12.447	11.766	11.039	10.767	0.081	0.048	0.061	1.03	-0.70
NGC 6266	V2	10.609	11.068	10.560	10.409	0.054	0.043	0.065	0.47	-1.29
NGC 6273	V1	16.920	11.357	10.873	10.736	0.030	0.028	0.029	0.41	-1.68
NGC 6273	V2	14.138	11.466	11.032	10.879	0.038	0.035	0.041	0.41	-1.68
NGC 6273	V4	2.433	13.225	12.770	12.684	0.026	0.026	0.043	0.41	-1.68
NGC 6284	V1	4.481	13.660	13.223	13.120	0.041	0.038	0.034	0.28	-1.32
NGC 6284	V4	2.819	14.111	13.663	13.605	0.037	0.038	0.042	0.28	-1.32
NGC 6293	V2	1.182	14.227	13.788	13.648	0.016	0.018	0.060	0.41	-1.92
NGC 6325	V1	12.516	11.985	11.275	11.053	0.037	0.038	0.038	0.89	-1.17
NGC 6325	V2	10.744	12.131	11.430	11.221	0.014	0.018	0.015	0.89	-1.17
NGC 6402	V1	18.743	11.558	11.033	10.834	0.026	0.042	0.048	0.60	-1.39
NGC 6402	V2	2.795	13.405	12.954	12.802	0.018	0.025	0.021	0.60	-1.39
NGC 6402	V7	13.599	12.035	11.468	11.303	0.033	0.021	0.026	0.60	-1.39
NGC 6402	V76	1.890	13.820	13.351	13.124	0.016	0.009	0.022	0.60	-1.39
NGC 6441	V129	17.832	12.146	11.593	11.471	0.022	0.103	0.068	0.47	-0.53
NGC 6441	V6	22.470	12.045	11.599	11.418	0.041	0.088	0.089	0.47	-0.53
NGC 6453	V1	31.070	11.470	10.812	10.632	0.037	0.026	0.026	0.66	-1.53
NGC 6453	V2	27.210	11.245	10.654	10.482	0.040	0.037	0.019	0.66	-1.53
NGC 6569	V16	87.500	10.502	9.669	9.422	0.105	0.084	0.085	0.55	-0.86
NGC 6626	V17	48.000	9.405	8.809	8.626	0.086	0.075	0.071	0.40	-1.45
NGC 6626	V4	13.458	10.757	10.190	10.047	0.055	0.046	0.062	0.40	-1.45
NGC 6749	V1	4.481	13.352	12.579	12.323	0.027	0.022	0.019	1.50	-1.60
NGC 6779	V1	1.510	13.993	13.631	13.553	0.016	0.040	0.058	0.20	-1.94
NGC 6779	V6	45.000	10.711	10.254	10.119	0.026	0.044	0.043	0.20	-1.94
NGC 7078	V86	16.800	11.665	11.261	11.155	0.039	0.035	0.030	0.10	-2.26
NGC 7089	V1	15.568	11.939	11.549	11.446	0.018	0.021	0.024	0.06	-1.62
NGC 7089	V11	33.400	10.860	10.479	10.401	0.060	0.037	0.042	0.06	-1.62
NGC 7089	V5	17.555	11.803	11.401	11.310	0.032	0.036	0.030	0.06	-1.62
NGC 7089	V6	19.360	11.665	11.291	11.204	0.030	0.038	0.042	0.06	-1.62
HP 1	V16	16.400	11.768	10.975	10.675	0.022	0.019	0.024	1.19	-1.50
HP 1	V17	14.420	11.872	11.062	10.783	0.044	0.041	0.040	1.19	-1.50
Ter 1	V5	18.850	11.960	10.921	10.578	0.026	0.027	0.035	2.28	-1.30

NOTE— $E_{BV} = E(B - V)$ .



**Table 11.** Type II Cepheid-based distance estimates for Galactic globular clusters

Cluster	$\mu(J)$	$\mu(H)$	$\mu(K_s)$	$\mu_{M06}$
NGC 1904	15.55±0.09	15.40±0.09	15.42±0.10	15.57
NGC 2808	15.01±0.09	15.27±0.09	15.05±0.11	14.90
NGC 5139	13.65±0.08	13.77±0.08	13.70±0.11	13.62
NGC 5272	14.89±0.07	15.01±0.07	14.95±0.07	15.10
NGC 5904	14.15±0.12	14.22±0.11	14.24±0.11	14.37
NGC 5986	15.20±0.06	15.03±0.06	15.05±0.07	15.11
NGC 6093	15.07±0.07	15.17±0.07	15.12±0.07	15.04
NGC 6218	13.64±0.08	13.68±0.06	13.62±0.08	13.45
NGC 6254	13.54±0.08	13.58±0.07	13.53±0.08	13.23
NGC 6256	14.12±0.10	14.24±0.07	14.18±0.08	14.57
NGC 6266	13.79±0.08	13.93±0.07	13.86±0.09	14.19
NGC 6273	14.55±0.07	14.73±0.06	14.65±0.07	14.71
NGC 6284	15.66±0.08	15.85±0.08	15.71±0.10	15.93
NGC 6293	14.75±0.09	15.04±0.09	14.76±0.13	14.76
NGC 6325	14.48±0.07	14.57±0.07	14.53±0.07	14.51
NGC 6402	14.73±0.07	14.95±0.08	14.82±0.09	14.86
NGC 6441	15.48±0.07	15.59±0.12	15.59±0.11	15.60
NGC 6453	14.94±0.07	14.98±0.07	15.03±0.07	14.93
NGC 6569	15.33±0.13	15.06±0.11	15.12±0.12	15.11
NGC 6626	13.77±0.10	13.77±0.10	13.76±0.10	13.74
NGC 6749	14.21±0.07	14.51±0.07	14.46±0.08	14.51
NGC 6779	15.07±0.08	15.22±0.09	15.12±0.12	15.08
NGC 7078	15.22±0.07	15.30±0.06	15.25±0.06	15.13
NGC 7089	15.36±0.06	15.43±0.07	15.41±0.07	15.33
HP 1	14.24±0.07	14.34±0.07	14.31±0.07	14.36
Ter 1	13.56±0.06	13.81±0.06	13.97±0.07	13.73

NOTE— $\mu_{M06}$ : derived by [Matsunaga et al. \(2006\)](#) based on magnitudes of horizontal branch stars.

use the absolute calibration of the LMC PLRs to determine distances to each T2C in Table 10 and compute weighted averages for clusters with more than one variable. The error budget includes uncertainties in: (1) mean magnitudes derived from template fits, (2) absolute calibration and (3) eclipsing binary distance to the LMC, added in quadrature. The results are presented in Table 11, along with the estimates by [Matsunaga et al. \(2006\)](#), who used the  $M_V - [\text{Fe}/\text{H}]$  relation. The bottom panel of Fig. 10 shows the difference between the two approaches; the distances are in agreement within  $2\sigma$  in almost all cases.

## 6. CONCLUSIONS

We summarize the results of this work as follows:

- We present time-series observations of 81 Type II Cepheids in the LMC at  $JHK_s$  wavelengths, based on the survey of [Macri et al. \(2015\)](#). The  $JK_s$  data complements the photometry from the VMC survey ([Ripepi et al. 2015](#)) while the  $H$ -band time-series observations are presented for the first-time. We develop templates using high-quality and well-sampled light curves of variables in the LMC (observed in  $I$ -band by OGLE) and the Galactic Bulge (observed in  $K_s$ -band by VVV).
- We derive robust mean magnitudes based on template fits and obtain Period-Luminosity relations for each class of variable. Our relations are consistent with published work based on variables in the LMC, Galactic globular clusters and the Galactic bulge.
- We compile near-infrared magnitudes for the entire sample of OGLE-III Type II Cepheids and derive new Period-Wesenheit relations by combining optical and near-infrared data. The slopes of the  $W_{V,K_s}$  and  $W_{V,J}$  relations are consistent with the findings of [Ripepi et al. \(2015\)](#); in the latter case, when the comparison is restricted to BL Hercules and W Virginis stars.
- We use the *Gaia DR1* parallax for VY Pyx and the *HST* parallaxes for  $k$  Pav and 5 RR Lyrae variables to obtain an absolute calibration of the zeropoint of the P-L relations. This yields an estimate of the LMC distance modulus of  $\mu_{\text{LMC}} = 18.54 \pm 0.08$  mag, in very good agreement with the more accurate and precise estimate by [Pietrzyński et al. \(2013\)](#). Our estimate is also consistent with recent results based on Classical Cepheids ([Monson et al. 2012](#); [Bhardwaj et al. 2016b](#)).
- We update the mean magnitudes for Type II Cepheids in 26 Galactic globular clusters using our light curve templates and estimate distances to these systems. Our findings are in good agreement with estimates based on horizontal branch stars by [Matsunaga et al. \(2006\)](#).

## ACKNOWLEDGMENTS

We thank the anonymous referee for his/her valuable comments which improved the content and quality of the manuscript. We are grateful to Noriyuki Matsunaga, Dante Minniti and Martino Romaniello for reading an earlier version of the manuscript and for useful comments. AB thanks the Council of Scientific and Industrial Research, New Delhi, India, for a Senior Research Fellowship. LMM acknowledges support by

the United States National Science Foundation through AST grant number 1211603 and by Texas A&M University through a faculty start-up fund and the Mitchell-Heep-Munnerlyn Endowed Career Enhancement Professorship in Physics or Astronomy. CCN thanks the funding from Ministry of Science and Technology (Taiwan) under the contract NSC104-2112-M-008-012-MY3. We acknowledge the use of data from the ESO Public Survey program ID 179.B-2002 taken with the VISTA telescope.

## REFERENCES

- Alcock, C., Allsman, R. A., Alves, D. R., et al. 1998, *AJ*, 115, 1921
- Benedict, G. F., McArthur, B. E., Feast, M. W., et al. 2011, *AJ*, 142, 187
- Bhardwaj, A., Kanbur, S. M., Macri, L. M., et al. 2016a, *MNRAS*, 457, 1644 (Paper III)
- . 2016b, *AJ*, 151, 88 (Paper II)
- Bhardwaj, A., Kanbur, S. M., Marconi, M., et al. 2016c, ArXiv e-prints, 1612.03806
- Bhardwaj, A., Kanbur, S. M., Singh, H. P., Macri, L. M., & Ngeow, C.-C. 2015, *MNRAS*, 447, 3342
- Bono, G., Caputo, F., & Santolamazza, P. 1997, *A&A*, 317, 171
- Borissova, J., Rejkuba, M., Minniti, D., Catelan, M., & Ivanov, V. D. 2009, *A&A*, 502, 505
- Cambridge Astronomy Survey Unit. 2016, VISTA Technical Information, Tech. rep., Institute of Astronomy, Cambridge University, <http://casu.ast.cam.ac.uk/surveys-projects/vista/technical/photometric-properties>
- Cardelli, J. A., Clayton, G. C., & Mathis, J. S. 1989, *APJ*, 345, 245
- Ciechanowska, A., Pietrzyński, G., Szewczyk, O., Gieren, W., & Soszyński, I. 2010, *Acta Astron.*, 60, 233
- Cioni, M.-R. L., Clementini, G., Girardi, L., et al. 2011, *A&A*, 527, A116
- de Grijs, R., Wicker, J. E., & Bono, G. 2014, *AJ*, 147, 122
- Feast, M. W., Laney, C. D., Kinman, T. D., van Leeuwen, F., & Whitelock, P. A. 2008, *MNRAS*, 386, 2115
- Groenewegen, M. A. T., Udalski, A., & Bono, G. 2008, *A&A*, 481, 441
- Haschke, R., Grebel, E. K., & Duffau, S. 2011, *AJ*, 141, 158
- Inno, L., Matsunaga, N., Romaniello, M., et al. 2015, *A&A*, 576, A30
- Kato, D., Nagashima, C., Nagayama, T., et al. 2007, *PASJ*, 59, 615
- Kubiak, M., & Udalski, A. 2003, *Acta Astron.*, 53, 117
- Leavitt, H. S., & Pickering, E. C. 1912, Harvard College Observatory Circular, 173, 1
- Lindgren, L., Lammers, U., Bastian, U., et al. 2016, *A&A*, in press, 1609.04303
- Lutz, T. E., & Kelker, D. H. 1973, *PASP*, 85, 573
- Macri, L. M., Ngeow, C.-C., Kanbur, S. M., Mahzooni, S., & Smitka, M. T. 2015, *AJ*, 149, 117 (Paper I)
- Madore, B. F. 1982, *ApJ*, 253, 575
- Madore, B. F., & Freedman, W. L. 1991, *PASP*, 103, 933
- Majaess, D., Turner, D., & Lane, D. 2009, *Acta Astron.*, 59, 403
- Matsunaga, N., Feast, M. W., & Menzies, J. W. 2009, *MNRAS*, 397, 933
- Matsunaga, N., Feast, M. W., & Soszyński, I. 2011, *MNRAS*, 413, 223
- Matsunaga, N., Fukushi, H., Nakada, Y., et al. 2006, *MNRAS*, 370, 1979
- Minniti, D., Lucas, P. W., Emerson, J. P., et al. 2010, *New Astronomy*, 15, 433
- Monson, A. J., Freedman, W. L., Madore, B. F., et al. 2012, *ApJ*, 759, 146
- Muraveva, T., Palmer, M., Clementini, G., et al. 2015, *ApJ*, 807, 127
- Nemec, J. M., Nemec, A. F. L., & Lutz, T. E. 1994, *AJ*, 108, 222
- Pietrzyński, G., Graczyk, D., Gieren, W., et al. 2013, *Nature*, 495, 76
- Riess, A. G., Macri, L. M., Hoffmann, S. L., et al. 2016, *ApJ*, 826, 56
- Ripepi, V., Moretti, M. I., Marconi, M., et al. 2015, *MNRAS*, 446, 3034
- Sandage, A., & Tammann, G. A. 2006, *ARA&A*, 44, 93
- Schmidt, E. G., Hemen, B., Rogalla, D., & Thacker-Lynn, L. 2009, *AJ*, 137, 4598
- Simon, N. R., & Lee, A. S. 1981, *ApJ*, 248, 291
- Sollima, A., Cacciari, C., & Valenti, E. 2006, *MNRAS*, 372, 1675

Soszyński, I., Gieren, W., & Pietrzyński, G. 2005, *PASP*, 117, 823

Soszyński, I., Udalski, A., Szymański, M. K., et al. 2010, *Acta Astron.*, 60, 91

—. 2008, *Acta Astron.*, 58, 293

Soszyński, I., Udalski, A., Pietrukowicz, P., et al. 2011, *Acta Astron.*, 61, 285

van Leeuwen, F. 2007, *A&A*, 474, 653

Wallerstein, G. 2002, *PASP*, 114, 689

White, H. 1980, *Econometrica*, 48, 817

## APPENDIX

## A. TEMPLATE-FIT LIGHT CURVES

The three panels of Figure 11 present the result of template fits to the  $JHK_s$  light curves of Type II Cepheids in the LMC based on data from Macri et al. (2015). Figure 12 shows the same, but for variables in Galactic globular clusters based on data from Matsunaga et al. (2006). Stars are arranged by decreasing period. The  $J$  (blue) and  $K_s$ -band (red) light curves have been offset by +0.25 and -0.5 mag for visualization purposes.  $H$ -band light curves are shown in violet color. The solid and dashed lines represent the best-fit  $I$ - and  $K_s$ -band based templates for each band. The star “ID” and “Period (in days)” are also provided on the top of each light curve.

The template-fits are performed using least-square minimization in *IDL MPCURVEFIT* routine. Templates can be used to  $JHK_s$  light curves with poor phase coverage in order to obtain robust mean-magnitudes. In case of single-epoch observations, accurate amplitude ratios for Type II Cepheids will be required to best-fit observations. For short-period Type II Cepheids, light curves exhibit large scatter with respect to the template-fits, which provide a robust estimate of the uncertainty associated with mean magnitudes.

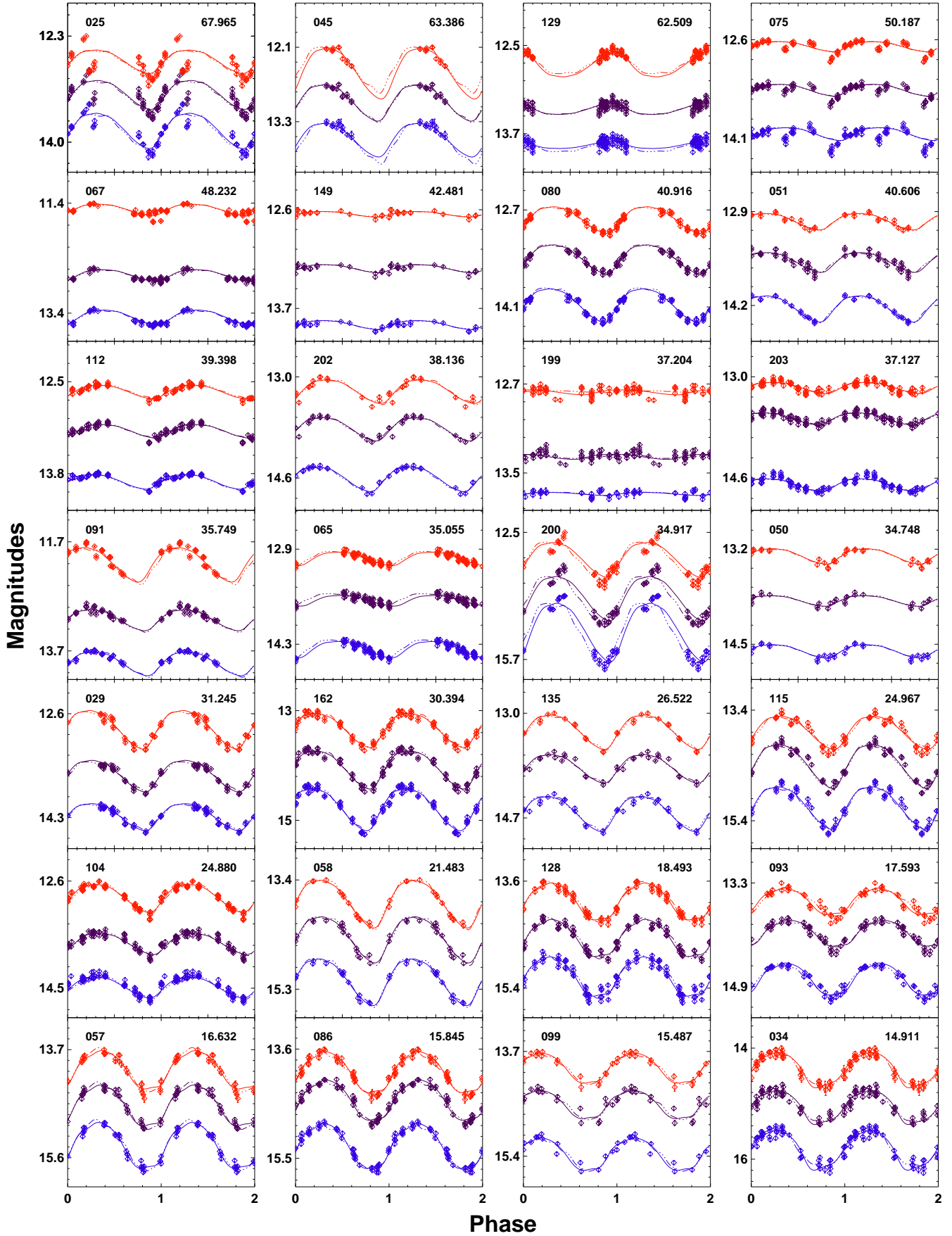


Figure 11. Template fits to light curves of Type II Cepheids in the LMC, based on data from [Macri et al. \(2015\)](#).

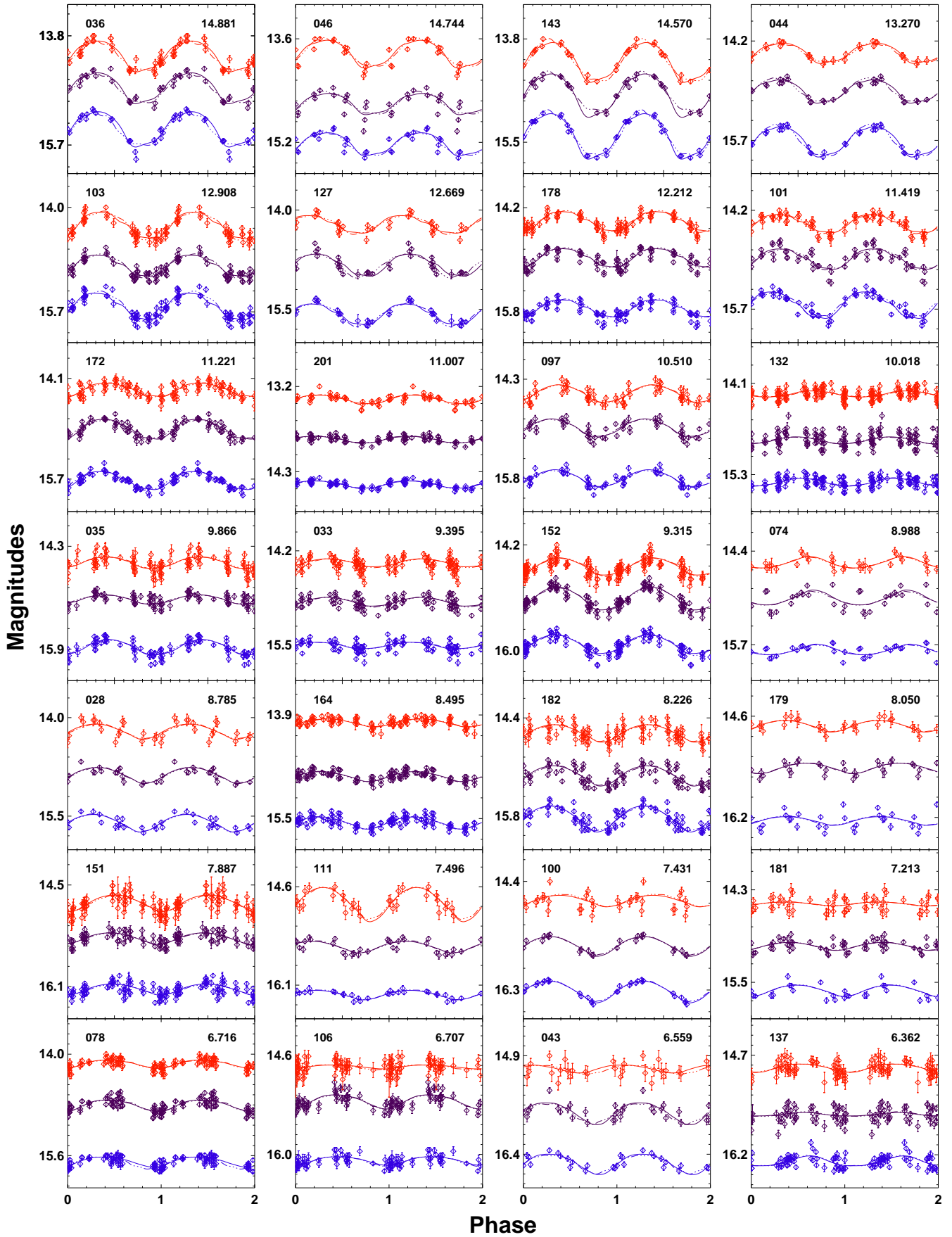


Figure 11. (continued).

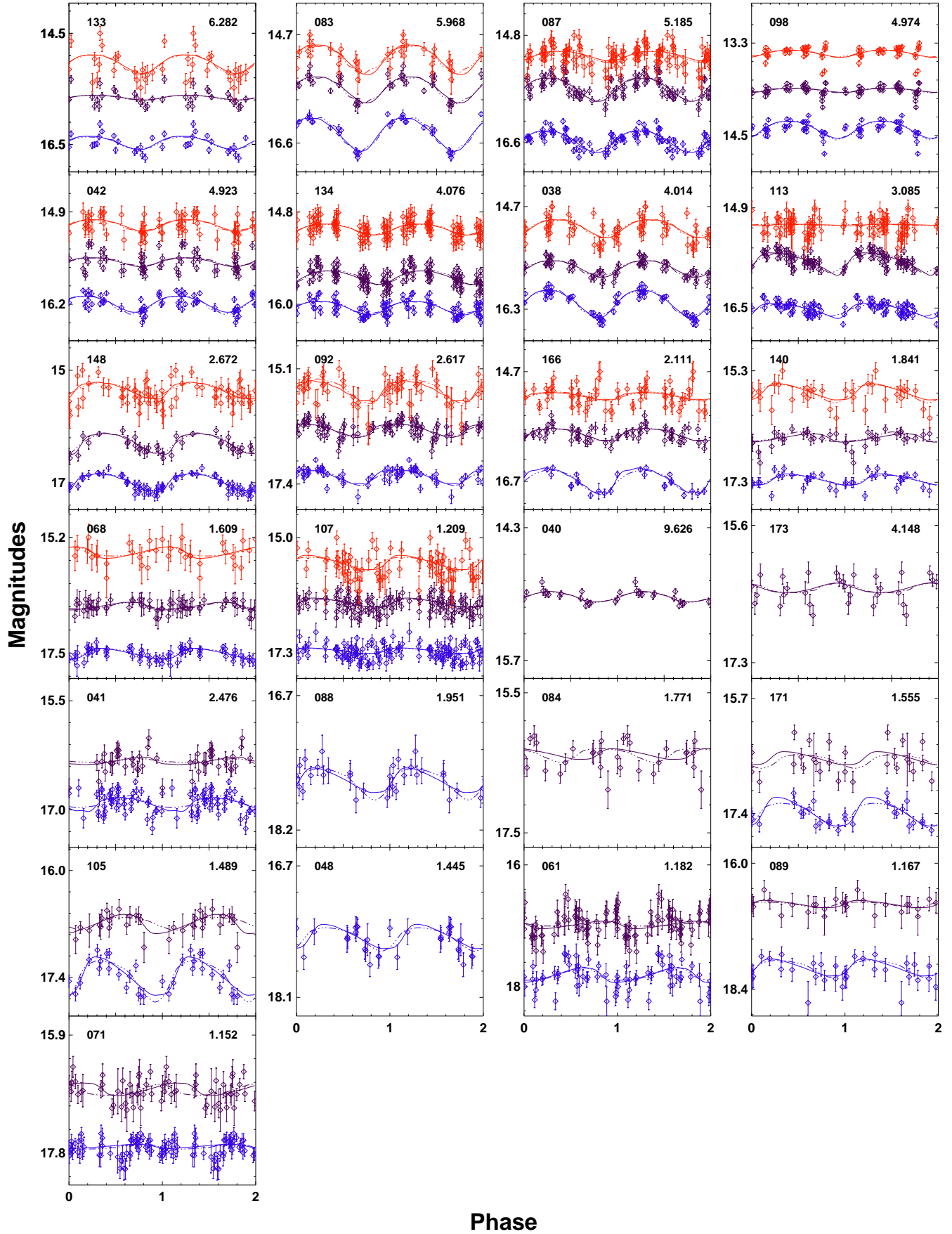


Figure 11. (continued).

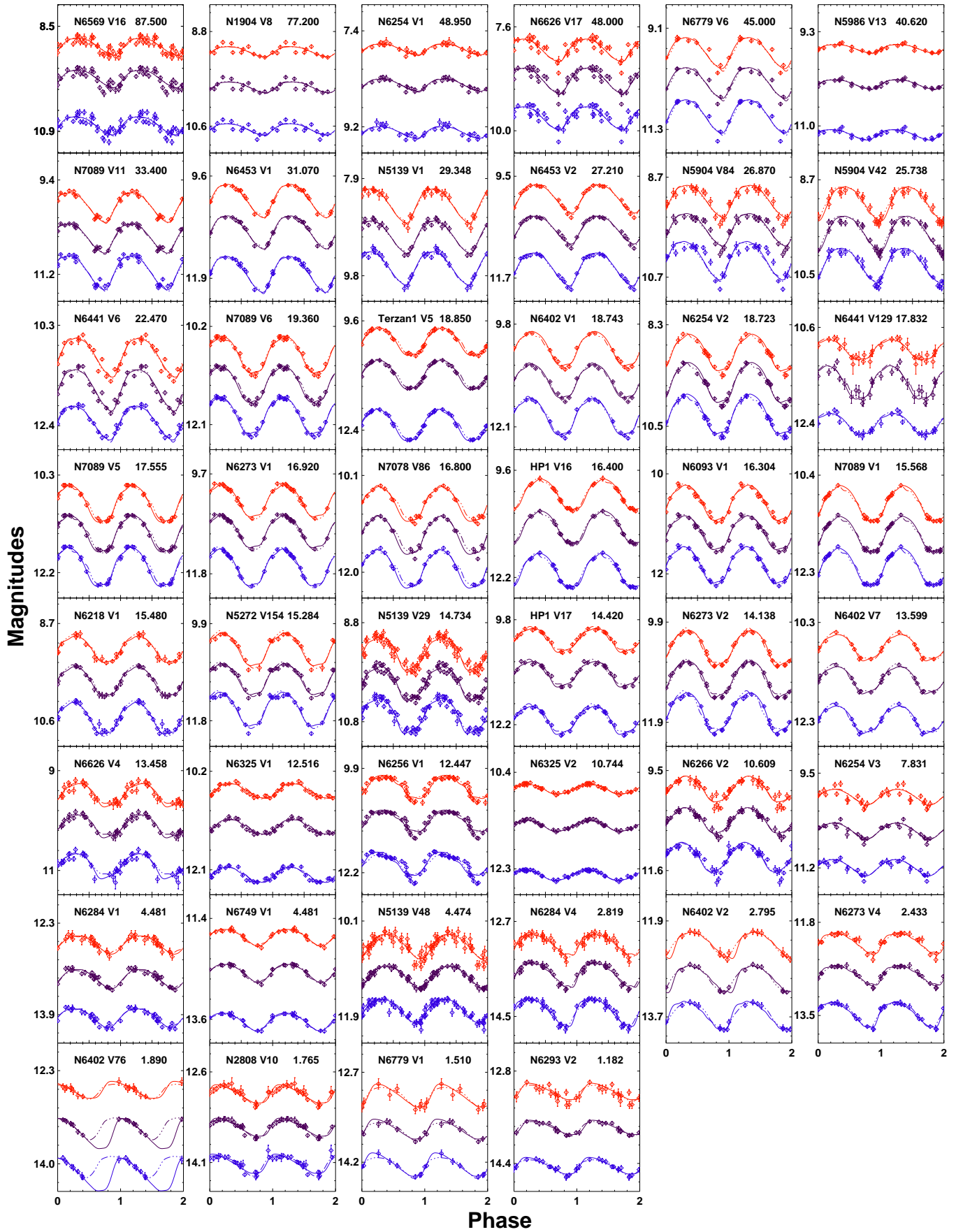


Figure 12. Template fits to light curves of Type II Cepheids in Galactic globular clusters, based on data from Matsunaga et al. (2006).